Geophys. J. R. astr. Soc. (1981) **65**, 103–128

A numerical model of flow over sand waves in water of finite depth

K. J. Richards* *Department of Applied Mathematics and Theoretical Physics, University of Cambridge, Silver Street, Cambridge CB3 9EW*

P. A. Taylor *Boundary Layer Research Division, Atmospheric Environment Service, Downsview, Canada*

Received 1980 May 19

Summary. A model of turbulent flow above sand waves in water of finite depth is described. Closure assumptions are based on an eddy viscosity proportional to the square root of the local value of turbulent kinetic energy and mixing length dependent upon distance from the lower boundary. Results are presented for some idealized cases to investigate the effects of wave slope, water depth, Froude number and wave shape. The implications of the model for the transport of sediment are discussed and the development of the wave investigated. It is found that the crest of the wave will become sharper for lower flow rates, as has been observed in the sea. Comparisons are made with recent measurements made over sand waves in the Columbia River.

Introduction

Sand waves, or dunes, commonly occur on a bed comprised of a non-cohesive sediment in both river and sea environments. The distribution and characteristics of these bed forms have been described by Allen (1968) and Taylor & Dyer (1977). The sand waves are often strikingly periodic and two-dimensional (see, e.g. Langeraar 1966).

The flow over a small amplitude perturbation to a flat erodible bed and the resulting stability of the bed has been investigated by Richards (1980) using a linear model for the flow.

In a series of papers, Taylor, Gent & Keen (1976), Gent & Taylor (1976), two-dimensional boundary-layer flow above gentle finite amplitude topography was studied numerically by the use of conformal mapping techniques. The bed-forms studied are restricted to those for which convenient conformal mappings can be found. To study the flow over an arbitrary topography Taylor (1977) extended this work by the use of a non-orthogonal transformation of the coordinate system. The above papers all deal with a deep turbulent boundary layer neglecting externally applied pressure gradients.

* Present address: Institute of Oceanographic Sciences, Wormley, Godalming, Surrey GU8 5UB.

Comparing results for flow over a sine wave obtained from the linear model of Richards (1980) with those of the non-linear model of Taylor (1977), Taylor, Richards & Nunes (1978) find that quantities such as the surface stress and pressure perturbations differ by about 25 per cent at wave slopes of 0.157 for the two solutions. There is agreement between the two models as the slope tends to zero. For slopes greater than 0.3 the solutions are often totally different. The linear model tends to overestimate the flow perturbations due to bed-waves of finite amplitude. In order to model the flow over a finite amplitude bed-wave and the corresponding sediment transport, it is therefore appropriate to use a fully non-linear model, although the numerical solution requires a far greater amount of computing time.

For sand waves occurring under natural flows the ratio of the wavelength to depth is approximately 2π and often greater. The effects of the finite depth to the flow will therefore be important. In this paper we will extend the work of Taylor (1977) to the case of open channel flow over a wavy bed of arbitrary shape.

The implications of the model for the development of the sand wave are investigated by relating the calculated bed shear stress distribution to the bed-load transport of sediment and thence to the local erosion/deposition rate. A preliminary study of this sort was carried out by Taylor & Dyer (1977) using the model of Taylor *et al.* (1976).

Finally the results of the model are compared with recent measurements reported by McLean (1976) of the flow above sand waves in the Columbia River.

2 Equations of motion and coordinate transformation

The flow considered is that of steady channel flow of depth D and inclination α to the horizontal above a periodic, two-dimensional, wavy surface ($z = z_b$) with wavelength L (see Fig. 1). In Cartesian coordinates the equations of motion are

$$U\frac{\partial U}{\partial x} + W\frac{\partial U}{\partial z} = -\frac{1}{\rho}\frac{\partial p}{\partial x} - \frac{\partial}{\partial x}\overline{u'^2} - \frac{\partial}{\partial z}\overline{u'w'} + g\sin\alpha \tag{2.1}$$

$$U\frac{\partial W}{\partial x} + w\frac{\partial W}{\partial z} = -\frac{1}{\rho}\frac{\partial p}{\partial z} - \frac{\partial}{\partial x}\overline{u'w'} - \frac{\partial}{\partial z}\overline{w'^2} - g\cos\alpha \tag{2.2}$$

$$\frac{\partial U}{\partial x} + \frac{\partial W}{\partial z} = 0 \tag{2.3}$$

where the coordinate system is defined in Fig. 1, U, W are the velocity components, p the pressure, g the acceleration due to gravity and $\overline{u'w'}$ etc. the Reynolds stresses.

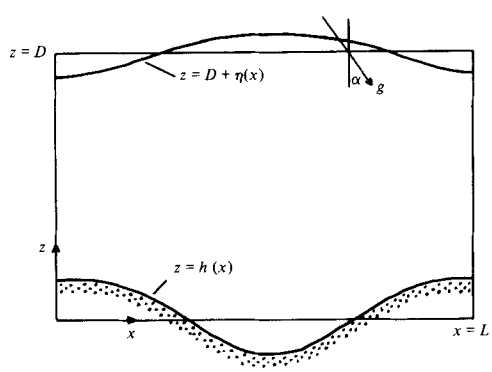

Figure 1. The flow considered.

The time-scale for the development of the bed-wave and, in the tidal situation, the tidal time-scale have been assumed to be long compared with the development time-scale of the flow. Richards (1980) has shown that these are reasonable assumptions although in some tidal flows in deep water this may not be strictly true. However, the majority of sediment transport will take place during the period of maximum shear stress when the flow will be close to a steady state.

The turbulence closure scheme is based on an isotropic eddy viscosity model as used by Taylor (1977). This takes the form

$$-\overline{u_i u_j} + \frac{2}{3} E \delta_{ij} = K \left(\frac{\partial u_i}{\partial x_j} + \frac{\partial u_j}{\partial x_i} \right) \tag{2.4}$$

where

$$E = \frac{1}{2} \sum_{i=1}^{3} \overline{u_i'^2}$$

is the mean turbulent kinetic energy per unit mass.

The eddy viscosity K is defined by

$$K = (\lambda E)^{1/2} l$$

where $1/\lambda$ is the equilibrium value of E/u_*^2 and u_* the friction velocity. The turbulent energy equation is required to determine the local value of E. The mixing length l is a prescribed function of position.

Britter, Hunt & Richards (1981) have shown that, although an eddy viscosity approach will give the correct results for the velocity components throughout the flow field and for the turbulence quantities close to the surface, at a distance s from the surface, where s is given by

$$s \ln s/z_0 = 2\kappa^2 L \tag{2.5}$$

z_0 is the surface roughness length and κ von Karman's constant, the history of the flow becomes important in determining the turbulent properties. For heights greater than s rapid distortion theory is found to give to a good approximation the changes in turbulence quantities. However, in determining the bed-load transport of sediment we require the bed shear stress and we expect the present model to give a reasonable estimate of its value.

To facilitate the numerical solution of the equations of motion over an arbitrary topography a non-orthogonal coordinate transformation is introduced. Full details are given in Taylor (1977). The coordinate system is transformed to a new system (x^*, z^*) defined by

$$\begin{aligned} x^* &= x \\ z^* &= z - z_b(x^*) F(z^*). \end{aligned} \tag{2.6}$$

The function F is chosen to set the lines $z^* =$ constant to be approximately streamlines and for the lines $z^* = 0$ and $z = D$ to correspond to the lower boundary and the undisturbed free surface respectively.

The potential flow solution suggests the use of

$$F(z^*) = \frac{\sinh k(D - z^*) - kDFr^2 \cosh k(D - z^*)}{\sinh kD - Fr^2 \cosh kD} \tag{2.7}$$

where $k = 2\pi/L$ and $Fr = U_0/\sqrt{gD}$ (U_0 is the undisturbed mean velocity at the surface). Note that on $z^* = 0$, $F = 1$ so that $z = z_b(x)$ and on $z^* = D$, $z = D + F(D)z_b$ which corresponds to the free surface predicted by the potential flow solution.

In addition the vertical coordinate z^* is transformed to ζ where

$$\zeta = \int_0^{z^*} \frac{\kappa}{l_0}\, dz'. \tag{2.8}$$

The local values of the mixing length, l, are specified as

$$l = l_0(z^*)G(x^*, z^*) \tag{2.9}$$

where $l_0(z^*)$ is the mixing length specified for a flat bottomed channel and

$$G = 1 + \exp(-kz^*)\left[\frac{l[(z - z_b)\cos\theta] - l(z^*)}{l(z^*)}\right]$$

is an empirical modification to take account of the non-orthogonality of the vertical coordinate and the bed. The angle θ is the slope of the bed, $\tan^{-1}(dz_b/dx)$.

The undisturbed mixing length $l_0(z)$ is taken to be

$$l_0 = \frac{\lambda_B \kappa (z + z_0)}{\lambda_B + \kappa (z + z_0)} \tag{2.10}$$

(*cf.* Blackadar 1962). For small z_0, l_0 tends to $\kappa(z + z_0)$ whilst for large z, l_0 tends to a constant value λ_B. We have taken $\lambda_B = D$. Various forms for l_0 have been tried (see Richards 1978), all of which give similar results provide $l_0 \sim \kappa(z + z_0)$ for small z. The transformed coordinate ζ is then given by

$$\zeta = \ln\frac{z^* + z_0}{z_0} + \frac{\kappa z^*}{\lambda_B}. \tag{2.11}$$

The equations in (x^*, ζ) space to be solved are the U momentum equation

$$U\frac{\partial U}{\partial x^*} + \left(U\frac{\partial z^*}{\partial x} + W\frac{\partial z^*}{\partial z}\right)\frac{\partial \zeta}{\partial z^*}\frac{\partial U}{\partial \zeta} = -\frac{\partial p_M}{\partial x^*} - \frac{\partial p_M}{\partial \zeta}\frac{\partial \zeta}{\partial z^*}\frac{\partial z^*}{\partial x} - g\cos\alpha\frac{\partial \eta}{\partial x} + 1.0 + D_1 \tag{2.12}$$

where D_1 represents the diffusive terms

$$D_1 = K\frac{\partial^2 U}{\partial x^{*2}} + K_{x^*}\frac{\partial U}{\partial x^*} + \frac{\partial \zeta}{\partial z^*}\frac{\partial}{\partial \zeta}\left(K\frac{\partial \zeta}{\partial z^*}\frac{\partial U}{\partial \zeta}\right)\left(\left[\frac{\partial z^*}{\partial x}\right]^2 + \left[\frac{\partial z^*}{\partial z}\right]^2\right)$$

$$+ 2K\frac{\partial^2 U}{\partial x^* \partial \zeta}\frac{\partial \zeta}{\partial z^*}\frac{\partial z^*}{\partial x} + K\frac{\partial \zeta}{\partial z^*}\frac{\partial U}{\partial \zeta}\left(\frac{\partial^2 z^*}{\partial x^2} + \frac{\partial^2 z^*}{\partial z^2}\right)$$

$$+ K_{x^*}\left(\frac{\partial U}{\partial \zeta}\frac{\partial z^*}{\partial x} - \frac{\partial W}{\partial \zeta}\frac{\partial z^*}{\partial z}\right)\frac{\partial \zeta}{\partial z^*} + \frac{\partial \zeta}{\partial z^*}\frac{\partial K}{\partial \zeta}\left(\frac{\partial U}{\partial x^*}\frac{\partial z^*}{\partial x} + \frac{\partial W}{\partial x^*}\frac{\partial z^*}{\partial z}\right),$$

the W momentum equation

$$U\frac{\partial W}{\partial x^*} + \left(U\frac{\partial z^*}{\partial x} + W\frac{\partial z^*}{\partial z}\right)\frac{\partial \zeta}{\partial z^*}\frac{\partial W}{\partial \zeta} = -\frac{\partial p_M}{\partial \zeta}\frac{\partial \zeta}{\partial z^*}\frac{\partial z^*}{\partial z} + D_2 \tag{2.13}$$

where

$$D_2 = K\frac{\partial^2 W}{\partial x^{*2}} + K_{x^*}\frac{\partial W}{\partial x^*} + \frac{\partial \zeta}{\partial z^*}\frac{\partial}{\partial \zeta}\left(K\frac{\partial \zeta}{\partial z^*}\frac{\partial W}{\partial \zeta}\right)\left(\left[\frac{\partial z^*}{\partial x}\right]^2 + \left[\frac{\partial z^*}{\partial z}\right]^2\right)$$
$$+ 2K\frac{\partial^2 W}{\partial x^* \partial \zeta}\frac{\partial \zeta}{\partial z^*}\frac{\partial z^*}{\partial x} + K\frac{\partial \zeta}{\partial z^*}\frac{\partial W}{\partial \zeta}\left(\frac{\partial^2 z^*}{\partial x^2} + \frac{\partial^2 z^*}{\partial z^2}\right)$$
$$+ K_{x^*}\left(\frac{\partial U}{\partial \zeta}\frac{\partial z^*}{\partial z} + \frac{\partial W}{\partial \zeta}\frac{\partial z^*}{\partial x}\right)\frac{\partial \zeta}{\partial z^*} + \frac{\partial \zeta}{\partial z^*}\frac{\partial K}{\partial \zeta}\left(\frac{\partial W}{\partial x^*}\frac{\partial z^*}{\partial x} - \frac{\partial U}{\partial x^*}\frac{\partial z^*}{\partial z}\right),$$

the continuity equation

$$\frac{\partial U}{\partial x^*} + \left(\frac{\partial U}{\partial \zeta}\frac{\partial z^*}{\partial x} + \frac{\partial W}{\partial \zeta}\frac{\partial z^*}{\partial z}\right)\frac{\partial \zeta}{\partial z^*} = 0, \tag{2.14}$$

and the turbulent energy equation

$$U\frac{\partial E}{\partial x^*} + \left(U\frac{\partial z^*}{\partial x} + W\frac{\partial z^*}{\partial z}\right)\frac{\partial \zeta}{\partial z^*}\frac{\partial E}{\partial \zeta} = K\left(\frac{\partial U}{\partial \zeta}\frac{\partial \zeta}{\partial x^*}\frac{\partial z^*}{\partial z} + \frac{\partial W}{\partial x^*} + \frac{\partial W}{\partial \zeta}\frac{\partial \zeta}{\partial z^*}\frac{\partial z^*}{\partial x}\right)^2$$
$$+ K\left(\frac{\partial U}{\partial x^*} + \frac{\partial U}{\partial \zeta}\frac{\partial \zeta}{\partial z^*}\frac{\partial z^*}{\partial x} - \frac{\partial W}{\partial \zeta}\frac{\partial \zeta}{\partial z^*}\frac{\partial z^*}{\partial z}\right)^2 + D_3 - \frac{(\lambda E)^2}{K} \tag{2.15}$$

where

$$D_3 = K\frac{\partial^2 E}{\partial x^{*2}} + K_{x^*}\frac{\partial E}{\partial x^*} + \frac{\partial \zeta}{\partial z^*}\frac{\partial}{\partial \zeta}\left(K\frac{\partial \zeta}{\partial z^*}\frac{\partial E}{\partial \zeta}\right)\left(\left[\frac{\partial z^*}{\partial x}\right]^2 + \left[\frac{\partial z^*}{\partial z}\right]^2\right)$$
$$+ 2K\frac{\partial^2 E}{\partial x^* \partial \zeta}\frac{\partial \zeta}{\partial z^*}\frac{\partial z^*}{\partial x} + K\frac{\partial \zeta}{\partial z^*}\frac{\partial E}{\partial \zeta}\left(\frac{\partial^2 z^*}{\partial x^2} + \frac{\partial^2 z^*}{\partial z^2}\right)$$
$$+ K_{x^*}\frac{\partial E}{\partial \zeta}\frac{\partial \zeta}{\partial z^*}\frac{\partial z^*}{\partial x} + \frac{\partial \zeta}{\partial z^*}\frac{\partial K}{\partial \zeta}\frac{\partial E}{\partial x^*}\frac{\partial z^*}{\partial x}.$$

We have set $p_M = (1/\rho)p + \frac{2}{3}E$ for convenience. The equations have been non-dimensionalized with respect to the friction velocity $u_* = (Dg \sin \alpha)^{1/2}$ and the depth, D.

3 Numerical method and boundary conditions

The equations (2.12)–(2.14) are solved in the region

$$0 \leqslant x^* \leqslant L, \quad 0 \leqslant z^* \leqslant D \left(\text{or } 0 \leqslant \zeta \leqslant \int_0^D \frac{\kappa}{l_0}\, dz'\right)$$

on a finite difference mesh with uniform grid spacing in x^* and ζ. The method used to solve the equations is based on the technique of artificial compressibility due to Chorin (1967) and is described in Gent & Taylor (1976). No details will be given here. This scheme was chosen in preference to the more efficient iterative scheme of Taylor *et al.* (1976) so that a top boundary condition can be specified on W rather than p. The iterative scheme used for the free-surface elevation (see below) requires this for stability. Another advantage of this technique is that separated flows can be considered. It should be noted, however, that once

separation has taken place we would expect the turbulence closure used in the model to be invalid. Nevertheless, the model should indicate the conditions under which separation is likely to take place, bearing in mind that separated flow solutions should be treated with caution.

Care is needed in the finite difference representation of the divergence and advection terms, to ensure conservation of mass and momentum. The schemes used are given in the Appendix.

At the lower boundary, $z^* = 0$, we will impose the conditions

$$U = W = 0, \qquad \frac{\partial E}{\partial n} = 0 \tag{3.1}$$

where $\partial/\partial n$ indicates a derivative normal to the lower boundary. The condition on E ensures no flux of turbulent energy through the lower boundary.

All of the results presented in detail are for $Fr = 0$, i.e. the upper surface is taken to be plane. Taking $Fr = 0$, the imposed upper boundary conditions on $z^* = D$ are

$$\frac{\partial U}{\partial z^*} = 0, \qquad W = 0, \qquad \frac{\partial E}{\partial z^*} = 0 \tag{3.2}$$

giving zero shear stress at the surface and zero flux of mass and turbulent energy through the surface.

A number of runs have been performed with non-zero Fr. The upper boundary was at $z^* = D$, the position of the free surface predicted by potential flow theory. The final computed position, $z = \eta_s$, was slightly displaced from this. Boundary conditions were still imposed at $z^* = D$ but we used the modified surface slope in the requirements $\partial U/\partial n = \partial E/\partial n = 0$ and $W = U \tan \partial \eta_s/\partial x$.

Lateral boundary conditions are of periodicity L in x^*, so that

$$U(0) = U(L), \qquad W(0) = W(L), \qquad E(0) = E(L) \qquad \text{and} \qquad p_M(0) = p_M(L).$$

In defining the coordinate transformation we need to specify the bed form, $z_b(x)$, and its first and second derivatives at points corresponding to both the U and W grid point positions across the wave. In applying the model to observed sand waves (see Section 6) the wave is fitted by a discrete number of data points. The U positions of $z_b(x_{2i})$ are specified and the W positions $z_b(x_{2i+1})$ are interpolated using a cubic fit. Derivatives are found using a five-point central differencing scheme. Thus we define

$$\frac{d}{dx} z_b(x_i) = \frac{1}{6\Delta x} [z_b(x_{i-2}) - 8z_b(x_{i-1}) + 8z_b(x_{i+1}) - z_b(x_{i+2})]$$

and

$$\frac{d^2}{dx^2} z_b(x_i) = \frac{1}{3\Delta x^2} [-z_b(x_{i-2}) + 16z_b(x_{i-1}) - 30z_b(x_i) + 16(x_{i+1}) - z_b(x_{i+2})]$$

where $\Delta x/2$ is the spacing between data points. Differences between the predicted shear stress distribution over a sine wave using the above representation of the bed wave and the analytical expression on a 20×14 grid where less than 0.1 per cent.

When the model was applied to a number of observed bed forms the converged solution exhibited an oscillation in the x direction of a two-grid point wavelength. This was overcome by filtering the original data of two-grid interval waves. Shapiro (1970) suggests a

two-pass filter of the form

$$\bar{Z}_i = \frac{Z_i}{2} + \frac{1}{4}(Z_{i-1} + Z_{i+1})$$
$$\bar{\bar{Z}}_i = \frac{3}{2}\bar{Z}_i - \frac{1}{4}(\bar{Z}_{i-1} + \bar{Z}_{i+1}). \tag{3.3}$$

The operator has the property of completely eliminating two-grid interval waves but with a minimum of damping of all longer waves. Successive applications of (3.3) filters longer and longer waves. Six applications of the filter reduced the amplitude of the oscillations to an acceptably small fraction of the total perturbation. In all but the most sharply crested waves, filtering was found to change all bed points by less than 2 per cent, a value usually well within the accuracy of the measurements.

For a typical run of the model we found that on a 10×10 grid a converged solution was reached after 2000 cycles taking 30 s CPU time on a CDC 7600 computer. Comparisons of the predicted bed shear stress using a 10×10 grid and a 20×14 grid showed a less than 1 per cent difference between the two results. The results presented for symmetric waves were obtained using a 10×10 grid. Those for asymmetric waves were on a 20×14 grid to increase the resolution on the steeper slope of the wave.

4 Results

Taylor *et al.* (1976) present the results of their model for a symmetric wave which is slightly sharper crested than a sine wave. Taylor (1977) presents the results for a sine wave. Both models are for a deep turbulent boundary layer. A comparison between the present numerical scheme and that of Taylor (1977) showed a less than 0.2 per cent difference between the results of the two models. We shall present only the results of the surface values of shear stress and pressure. The flow above the bed for a finite depth flow is qualitatively similar to that shown in Taylor *et al.* (1976).

The model depends on the four parameters, Fr, D/z_0, L/D, a/z_0 and the shape of the wave, where a is the amplitude of the wave. Within a limited amount of computing resources it is not possible to span the whole parameter space. However, in the following an attempt is made to demonstrate some of the effects of the various parameters. Note that except in Section 4.3 the Froude number, Fr, is taken to be zero.

4.1 EFFECTS OF VARIATION IN DEPTH, AMPLITUDE AND ROUGHNESS

The shape of the wave for the results presented in this section is always a sine wave, i.e. $z_b = a \cos kx$.

To assess the effects of varying the depth of flow on the model a series of computations were performed keeping the dimensions of the bed-wave constant, with $L/z_0 = 10\,000$ and $a/z_0 = 250$ and varying L/D. The bed shear stress for varying L/D is shown in Fig. 2.

The infinite depth case (similar to Taylor 1977) shows the maximum in the bed shear stress to be upstream of the wave crest with a phase of $-25°$. A noticeable feature of the effect of decreasing the depth of flow is that the maximum value of the bed shear stress, τ_{max}, increases and the minimum, τ_{min}, decreases with a sharpening of the curve at the maximum. The phase of the maximum relative to the crest is decreased. There is roughly a 30 per cent increase in the value of the perturbed maximum from $D \to \infty$ to $L/D = 6.25$. With $L/D = 25$ the flow separates about half way down the lee slope with the stress

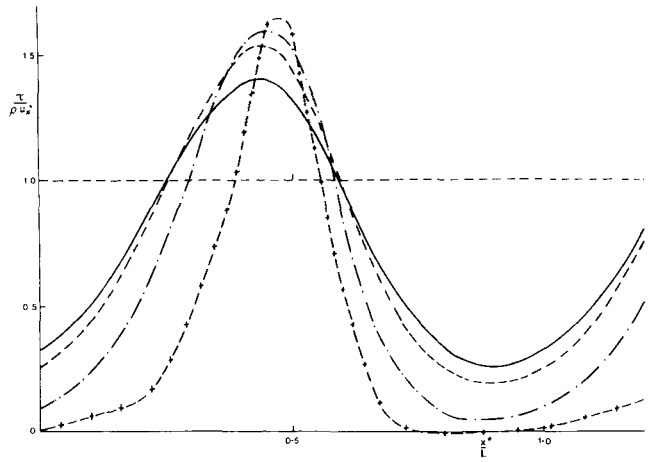

Figure 2. Bed shear stress distribution for varying depth of flow over a sine wave; $L/z_0 = 10\,000$, $a/z_0 = 250$: ——, $D \to \infty$; – – –, $L/D = 6.25$; – . –, $L/D = 12.5$; – + –, $L/D = 25.0$.

becoming negative. The values of the bed extrema of stress and pressure and their phases relative to the crest are given in Table 1. The value of the integrated shear stress along the wave $\langle \tau_x \rangle$ decreases significantly with increasing L/D, with the skin friction only accounting for 39 per cent of the total drag when $L/D = 25$, the remainder being due to form drag.

Table 1. Effects of depth variation; $L/z_0 = 10\,000$, $a/z_0 = 250$, sine wave.

	Surface shear stress				Surface pressure		
L/D	τ_{max}	τ_{min}	Phase of* τ_{max} (°)	$\langle \tau \rangle$	p_{max}	p_{min}	Phase of* p_{max} (°)
∞	1.40	0.26	−25	0.74	23.5	−30.0	187
6.25	1.55	0.18	−23	0.73	25.9	−32.4	184
12.5	1.59	0.04	−18	0.61	27.2	−39.5	180
25.0	1.65	−0.01	−9	0.39	19.1	−38.4	155

* Phase relative to crest of bed wave. Stresses are scaled with respect to u_*^2.

Table 2. Effects of amplitude variation; $D/z_0 = 1600$, $L/D = 6.25$, sine wave.

		Surface shear stress				Surface pressure		
a/k	a/z_0	τ_{max}	τ_{min}	Phase of* τ_{max} (°)	$\langle \tau \rangle$	p_{max}	p_{min}	Phase of* p_{max} (°)
0.063	100	1.34	0.63	−29	0.96	15.8	−16.8	193
0.094	150	1.47	0.46	−26	0.90	20.4	−24.0	187
0.126	200	1.54	0.31	−24	0.82	23.9	−29.0	185
0.157	250	1.55	0.18	−23	0.73	25.9	−32.4	184
0.188	300	1.50	0.10	−22	0.64	26.5	−34.6	182
0.220	350	1.44	0.04	−20	0.56	25.7	−36.8	181
0.251	400	1.37	0.00	−19	0.47	24.0	−35.9	176
0.283	450	1.29	−0.02	−18	0.40	21.6	−33.7	169
0.314	500	1.18	−0.04	−16	0.33	19.3	−31.1	162

* Phase relative to crest of bed wave. Stresses and scaled with respect to u_*^2.

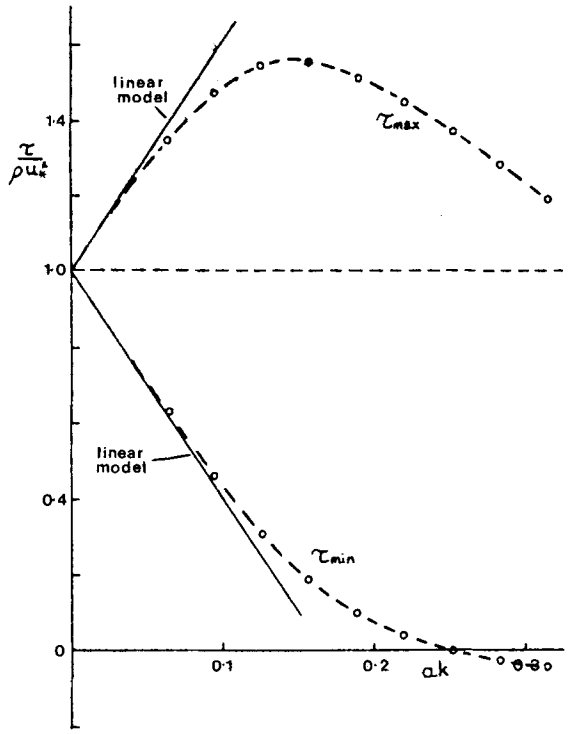

Figure 3. Variation of maximum and minimum values of the bed shear stress with wave slope for a sine wave; $D/z_0 = 1600$, $L/D = 6.25$: $-\circ-$, numerical non-linear model; ——, linear model (Richards 1980).

The results for fixed values of $L/D = 6.25$ and varying amplitude are given in Table 2 with the stress maximum and minimum plotted against ak (the maximum wave slope) in Fig. 3. Also shown in Fig. 3 are results of the linear model of Richards (1980). For low values of ak, τ_{max} and τ_{min} tend to a linear function of ak as predicted by the linear model. At larger values of ak the results of the non-linear model depart from those predicted by the linear model with the linear model overpredicting the effect of the wave. τ_{max} attains a maximum value at approximately $ak = 0.14$ decreasing significantly with ak above this value. τ_{min} decreases with increasing ak with the flow separating at approximately $ak = 0.25$.

Table 3. Effects of surface roughness variation; $a/L = 0.025$, $L/D = 6.25$, sine wave.

	Surface shear stress				Surface pressure		
D/z_0	τ_{max}	τ_{min}	Phase of* τ_{max} (°)	$\langle\tau\rangle$	p_{max}	p_{min}	Phase of* p_{max} (°)
160	1.66	0.18	−27	0.77	11.0	−14.1	174
800	1.58	0.18	−24	0.74	20.5	−26.8	180
1600	1.55	0.18	−23	0.73	25.9	−32.4	184
4000	1.49	0.21	−22	0.72	34.3	−43.5	187
8000	1.44	0.22	−20	0.72	41.4	−54.2	192
16 000	1.40	0.23	−18	0.71	48.7	−61.9	195

* Phase relative to crest of bed wave. Stresses scaled with respect to u_*^2.

Fig. 2 indicates that we would expect the flow to separate at a smaller value of ak for a larger value of L/D. With $L/D = 12.5$ the flow was found to separate at a wave slope of $ak = 0.17$.

Finally the effect of the surface roughness was investigated by fixing ak at 0.157 and L/D at 6.25 and varying D/z_0. The results are given in Table 3. No significant change occurs in the maximum and minimum values of the bed shear stress over two orders of magnitude variation in z_0, the range in the surface values decreasing for the smoother surfaces.

4.2 EFFECTS OF VARIATION IN SHAPE

Sand waves observed in the field differ in shape to the idealized sine wave used in the preceding sections. Waves formed by a symmetric tidal current (i.e. with equal and opposite ebb and flood currents) are more trochoidal in appearance with a sharper crest, whereas those formed by a unidirectional current or by an asymmetric tidal current are asymmetric with a shallow stoss slope and steeper lee slope, the asymmetry being in the direction of the dominant tidal stage for tidal flows (see, e.g. Van Veen 1935).

In order to illustrate the effects of changes in wave shape three different bed forms will be considered:

(1) a sine wave $z_b = a \cos kx$ (4.1)

(2) a $\sin^4$ wave $z_b = a\left(2 \sin^4\left(\frac{kx}{2}\right) - 1\right)$ (4.2)

and

(3) $z_b = -a \cos (kx + c_3(1 - \cos (kx + c_2(1 - \cos (kx + c_1(1 - \cos (kx)))))))$ (4.3)

with

$c_1 = -\pi/12, \quad c_2 = -\pi/8, \quad c_3 = -\pi/4.$

Waves (2) and (3) are the same as those used by Taylor *et al.* (1977) and their profiles are shown in Fig. 4. Wave (2) is a symmetrical wave with a sharper crest than the sine wave. Useful wave forms using the expression (3) were found by trial and error. With the given parameters the wave is asymmetric with smooth stoss and lee slopes. Unfortunately no way was found arbitrarily to specify the degree of asymmetry of the wave. Because of the steepness of the slopes computations were performed on a 20×14 grid.

Results were obtained for waves (2) and (3) with fixed $D/z_0 = 1600$ and $L/D = 6.25$ and varying a/z_0 (see Tables 4 and 5). The results for the three waves of bed shear stress and pressure are compared in Fig. 4. The distributions of bed pressure show no major changes for different wave shapes except that they reflect the shape of the underlying wave. The maximum and minimum values and the phase relative to the bed wave varies little. The distributions of bed shear stress again reflect the shape of the bed wave. However, there is a singnificant increase in the maximum value of the waves (2) and (3), there being an increase of approximately 63 per cent in the perturbed values of τ_{max} between waves (1) and (2). The phases of τ_{max} relative to the crest also varies, it being $-23°$, $-15°$ and $-6°$ for the three waves respectively. The contributions of the form drag of the different waves to the total stress varies but perhaps less than would be expected. They are 27, 35 and 37 per cent respectively.

The wave height at which the flow will separate varies with wave shape. The value of ak at which this happens was found to be 0.25, 0.22 and 0.15 for the three waves respectively, the asymmetric wave separating at the smaller value of ak.

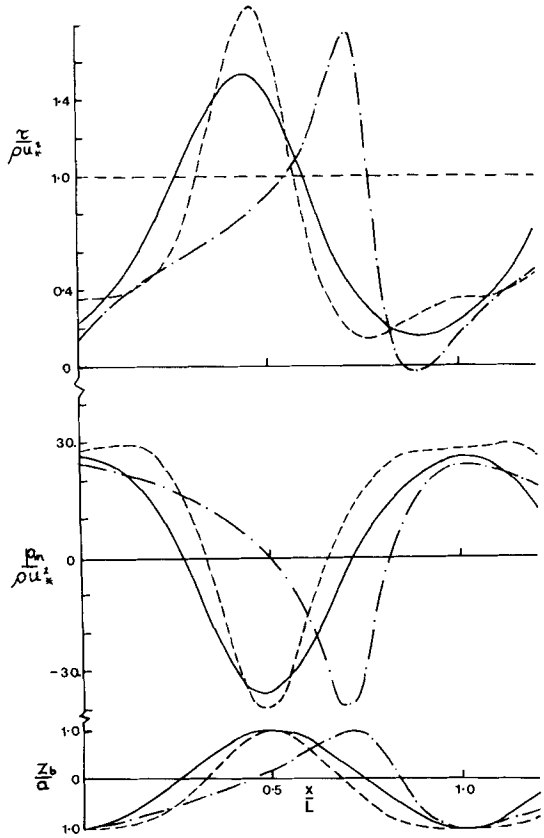

Figure 4. Distribution of bed shear stress for various wave shapes: $D/z_0 = 1600$, $a/z_0 = 250$, $L/D = 6.25$: ——, wave (1) (equation 4.1); – – –, wave (2) (equation 4.2); – · –, wave (3) (equation 4.3).

In the tidal situation the flow will be in both directions over the wave. In the case of the asymmetric wave we will therefore require the results of the flow over the wave in the reverse direction against the asymmetry. The results for the bed shear stress and pressure for each case are given in Fig. 5 where $D/z_0 = 1600$, $a/z_0 = 250$ and $L/D = 6.25$. The maximum shear stress occurs a little way down the steeper slope and the perturbed value is approximately 60 per cent larger than that for the flow in the opposite direction (Fig. 4). The stress

Table 4. Effects of shape variation; $D/z_0 = 1600$, $L/D = 6.25$, $\sin^4$ wave.

		Surface shear stress						Surface pressure		
ak	a/z_0	α_{max}	τ_{max}	τ_{min}	Phase of* τ_{max} (°)	$\langle\tau\rangle$	$\langle z_b\rangle$	p_{max}	p_{min}	Phase of* p_{max} (°)
0.126	200	0.163	1.84	0.29	16	0.78	−0.031	26.8	−36.0	220
0.157	250	0.204	1.88	0.15	15	0.68	−0.039	29.9	−39.2	221
0.188	300	0.245	1.85	0.06	14	0.57	−0.047	31.7	−39.6	222
0.220	350	0.286	1.76	0.00	14	0.46	−0.055	32.6	−38.1	222
0.251	400	0.326	1.61	−0.03	13	0.37	−0.063	32.2	−33.8	223
0.283	450	0.367	1.42	−0.05	12	0.29	−0.070	31.7	−28.2	223

* Phase relative to crest of bed wave. Stresses scaled with respect to u_*^2.

Table 5. Effects of shape variation; $D/z_0 = 1600$, $L/D = 6.25$, wave (3).

		Surface shear stress						Surface pressure		
ak	a/z_0	α_{max}	τ_{max}	τ_{min}	Phase of* τ_{max} (°)	$\langle\tau\rangle$	$\langle z_b\rangle$	p_{max}	p_{min}	Phase of* p_{max} (°)
0.126	200	0.260	1.75	0.09	7	0.76	−0.019	23.5	−36.5	175
0.157	250	0.325	1.76	−0.02	6	0.64	−0.023	24.2	−39.0	182
0.188	300	0.390	1.69	−0.08	5	0.52	−0.028	24.0	−36.2	190
0.220	350	0.455	1.53	−0.12	5	0.40	−0.033	22.2	−32.2	198
0.251	400	0.520	1.37	−0.14	4	0.30	−0.037	20.5	−26.0	216
0.283	450	0.585	1.20	−0.16	3	0.23	−0.042	19.7	−21.2	230

* Phase relative to crest of bed wave. Stresses scaled with respect to u_*^2.

minimum has been decreased and the flow does not separate. Rather surprisingly the form drag, 30 per cent of the total is little different from that for the flow with the asymmetry, 26 per cent.

4.3 EFFECTS OF VARIATION IN FROUDE NUMBER

The computation scheme devised for non-zero Froude number was not entirely satisfactory and was only convergent for $Fr \lesssim 0.5$. Typical values in marine and deep river situations will, however, be lower than this (say $\lesssim 0.1$) and for these cases we have found only small variations from the $Fr = 0$ results. For our basic sine wave bed-form with $D/z_0 = 1600$, $L/D = 6.25$ and with $ak = 0.157$ bed shear stress results for $Fr = 0.25$ agreed with those for $Fr = 0$ to within about $0.02u_*^2$ while for $Fr = 0.5$ the amplitude of the stress perturbation was increased by about $0.1u_*^2$. Free surface displacements for $Fr = 0.25$ are about $0.05a$, slightly smaller than, and advanced slightly in phase from the irrotational flow prediction. In general, Froude number variation effects were found to be small for $Fr \lesssim 0.25$ and have not been considered in the sediment transport calculations.

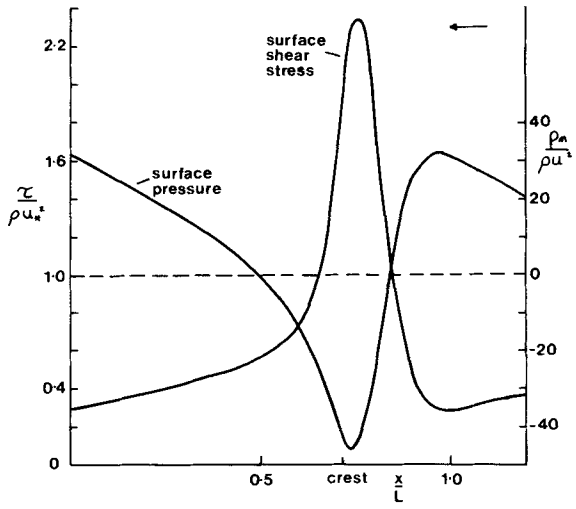

Figure 5. Bed shear stress and bed pressure distributions for flow right to left across the asymmetric wave (3); $D/z_0 = 1600$, $a/z_0 = 250$, $L/D = 6.25$.

5 Implications of the model for sediment transport

We shall assume that the sediment is transported as bed load only, thus restricting the present results to low shear rates. The sediment transport can then be related to the local bed shear stress. Bagnold (1966) balanced the rate of work done in pushing the bed load along the bed against a frictional resistance with the fluid power. For a bed of local slope α' this gives the bed-load transport of sediment q_b as

$$q_b = \frac{8.5}{\gamma g} \frac{e_b \tau^{3/2}}{(\tan \phi + \tan \alpha') \cos \alpha'} \tag{5.1}$$

where e_b is an efficiency factor of order 0.1 and varies slightly with flow velocity and grain size, ϕ is the angle of frictional resistance and $\gamma = (\rho_s - \rho)/\rho$, ρ_s being the density of the sediment. We have followed Inman (1963) and taken the fluid power as $\tau^{3/2}$. This assumes that the majority of sediment transport during a tidal cycle takes place when $\tau \gg \tau_c$, the critical shear stress for sediment movement. Clearly this is not so when the flow is close to or separating. However, if the fluid power is taken as $\tau^{1/2}(\tau - \tau_{cr})$ we find that there is a singularity in the erosion rate, which is proportional to $\partial q_b/\partial x$, at $\tau = \tau_{cr}$ unless either $\tau_{cr} = 0$ or $\partial \tau/\partial x = 0$ which in general they are not. In reality such a large build-up of sediment would be smoothed out by the flow. We will restrict ourselves in this section to studying bed forms with non-separating flows.

From experimental data Bagnold (1954) finds that $\tan \phi$ varies from 0.32, when the stresses in the moving sediment layer are transmitted totally inertially, to 0.75, when the stresses are transmitted viscously. Tan ϕ decreases for increasing shear stress and grain size. We shall consider two cases with $\tan \phi = 0.3$ (relatively high shear) and 0.6 (low shear).

Taylor & Dyer (1977) find that if the efficiency factor e_b is allowed to be variable and a function of τ, the width of the erosion and deposition zones predicted will be altered, and the rate of heightening of the sand wave either increased or decreased depending on whether e_b decreases or increases with τ, respectively. For convenience we will choose to take e_b as a constant over the wave bearing in mind that our results may be altered slightly for a varying e_b.

The growth rate of the bed $\partial z_b/\partial t$ can be related to the local bed-load transport using the sediment continuity equation due to Exner (1925). Thus

$$\frac{\partial q_b}{\partial x} = -(1-n)\frac{\partial z_b}{\partial t} \tag{5.2}$$

where n is the porosity of the bed.

The bed shear stress predicted by the numerical model for a sinusoidal bed wave with $D/z_0 = 1600$, $L/D = 6.25$ and $a/z_0 = 250$ is shown in Fig. 6(a). This wave has a steepness $(2a/L)$ of 1/20. The maximum shear stress occurs 23° upstream of the crest. The resulting bed-load transport rate, q_b/e_b, is shown in Fig. 6(b), taking $\tan \phi = 0.6$. The effect of including the local bed slope, $\tan \alpha'$, in the transport formula (equation 5.1) is to decrease the phase lag of the maximum transport rate to 12 per cent. This decrease in the phase lag is dependent on the value of $\tan \phi$, it being greater for smaller values of $\tan \phi$.

The non-dimensional growth rate

$$\sigma = -\frac{z_0 \gamma g (1-n)}{e_b u_*^3}\left(\frac{\partial z_b}{\partial t}\right) \tag{5.3}$$

calculated from equation (5.2) is shown in Fig. 6(c). Maximum erosion occurs approximately 34° upstream of the crest and maximum deposition about 22° downstream of the

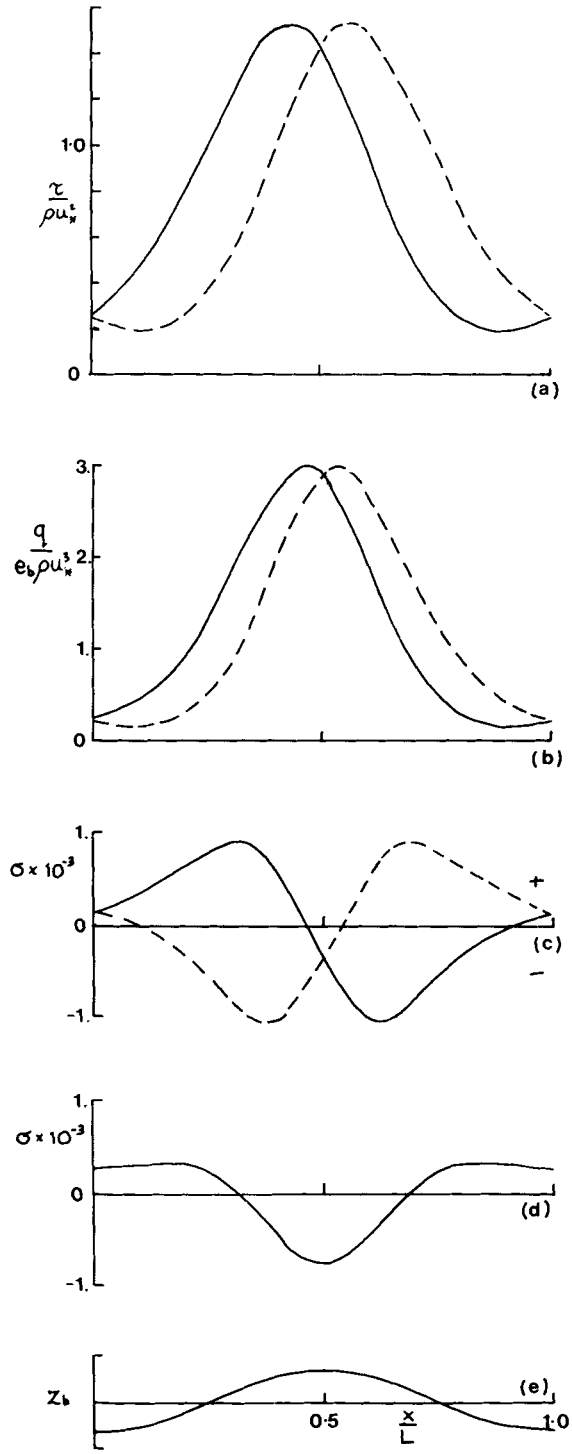

Figure 6. Bed shear stress and bed load transport for flow in opposite directions over a sine wave; $D/z_0 = 1600$, $L/D = 6.25$, $a/z_0 = 250$, $\tan\phi = 0.6$. Solid line, flow left to right, broken line, flow right to left. (a) Shear stress distribution; (b) bed load transport rates; (c) erosion rate; (d) net erosion rate over tidal cycle; (e) wave shape.

crest. In a unidirectional flow this would lead to a forward translation of the wave with the wave developing a steeper lee slope. The flow in the opposite direction across the sand wave produces a mirror image distribution about the crest. The net erosion over a tidal cycle with flood and ebb currents of equal magnitude is shown in Fig. 6(d). Deposition occurs within about 38° either side of the crest with a maximum at the crest. The maximum erosion occurs at 57° either side of the crest. This would lead to a sharpening of the crest and a flattening of the trough with the bed form assuming a more trochoidal form. Similar shaped curves for the net erosion were obtained for all values of a/z_0 ($\leqslant 500$) considered and for $\tan\phi = 0.3$ with the wave becoming steeper in each case.

The bed load and erosion curves for the $\sin^4$ wave (wave (2), equation 4.2) with $D/z_0 = 1600$, $L/D = 6.25$ and $a/z_0 = 250$ are shown in Figs 7 and 8 with $\tan\phi = 0.6$ and 0.3 respectively. The shape of the erosion curve with $\tan\phi = 0.6$ is similar to that for wave (1). Again the net effect over a tidal cycle would be for the wave to assume a more trochoidal form. The rate of heightening of the crest is approximately 1.5 times that for wave (1).

With $\tan\phi = 0.3$, however, the maximum in the bed load is 2° downstream of the crest with the consequence that over half a tidal cycle the erosion rate at the crest is positive and

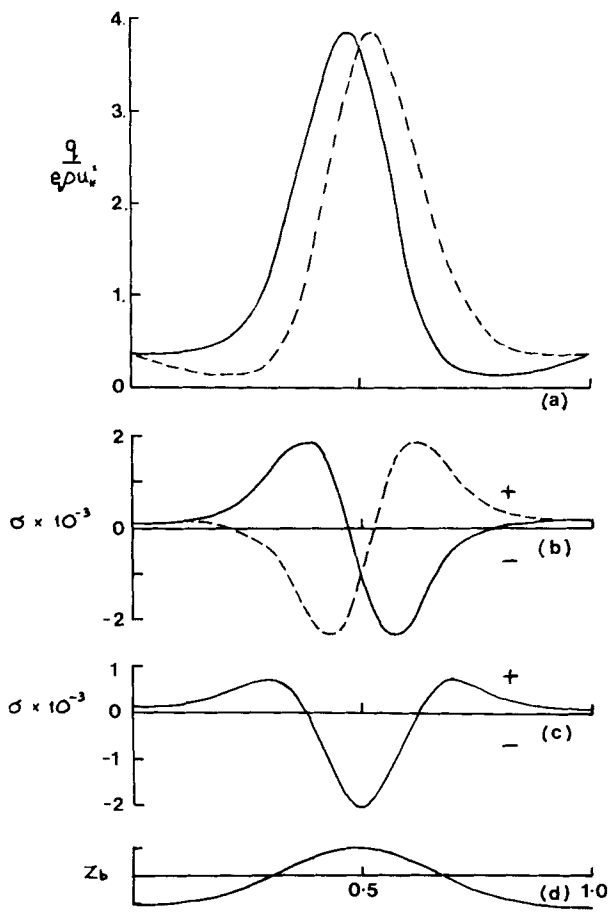

Figure 7. Bed load transport over $\sin^4$ wave; $D/z_0 = 1600$, $L/D = 6.25$, $a/z_0 = 250$, $\tan\phi = 0.6$. Solid line flow left to right; broken line, flow right to left. (a) Bed load transport rates; (b) erosion rates; (c) net erosion over tidal cycle; (d) wave shape.

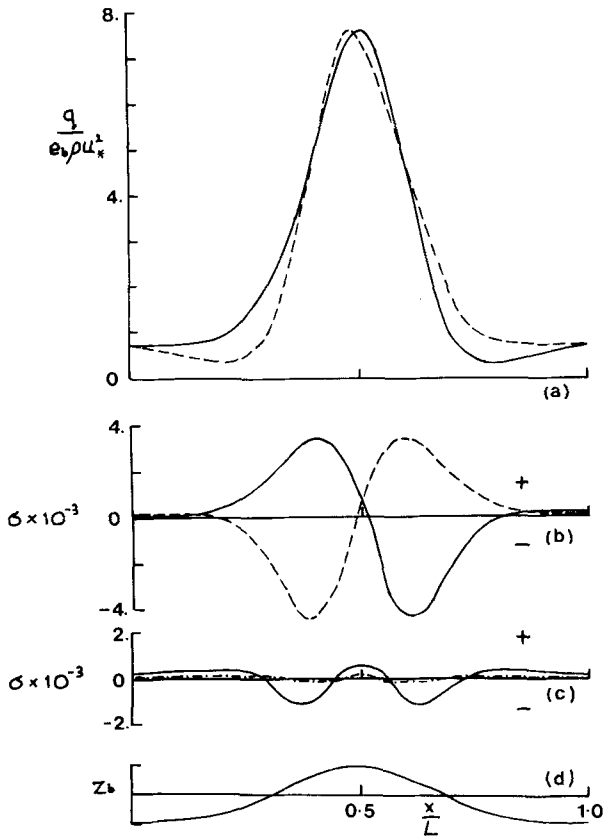

Figure 8. Bed load transport over $\sin^4$ wave. As for Fig. 7 with $\tan\phi = 0.3$. In (c): $-\cdot-$, $a/z_0 = 200$.

the crest height decreases with time. The net erosion over a tidal cycle is shown in Fig. 8(c). Erosion occurs over the crest and to 10° either side. Deposition occurs in a zone 10° to 60° with a small amount of erosion over the rest of the wave. This would result in the wave becoming flatter at the crest and slightly steeper in the lower flanks of the wave.

Also shown in Fig. 8(c) is the net erosion curve obtained with $a/z_0 = 200$ ($2a/L = 1/25$). The net erosion is nearly zero over the wave with a small amount of erosion at the crest.

The bed wave will become stable, i.e. remain unchanged from one tidal cycle to the next, when the net erosion is zero over the entire wave. The above results suggest that the shape of the stable bed form is dependent on the value of $\tan\phi$. For $\tan\phi = 0.3$ the wave form will be slightly flatter crested than the $\sin^4$ wave with a value for the steepness of about 1/25. This compares with a typical value of 1/30 for observed sand waves (see Taylor & Dyer 1977). For higher values of $\tan\phi$ the wave will be sharper crested. For $\tan\phi = 0.6$ we are unable from the present results to predict the steepness of the stable bed form which will have a crest somewhat sharper than that of the $\sin^4$ wave.

The results for the sediment transport over an asymmetric wave (wave (3), equation 4.3) are shown in Figs 9 and 10 with $\tan\phi = 0.6$ and 0.3 respectively. We have taken $D/z_0 = 1600$, $L/D = 6.25$ and $a/z_0 = 200$ which gives a wave of steepness 1/25 with a maximum wave slope of 0.16. The erosion curve with $\tan\phi = 0.6$ (Fig. 9b) shows deposition occurring at the crest and on the lee slope with erosion on the stoss slope. In a uni-directional flow the wave will become sharper crested and the lee slope steeper with the crest height

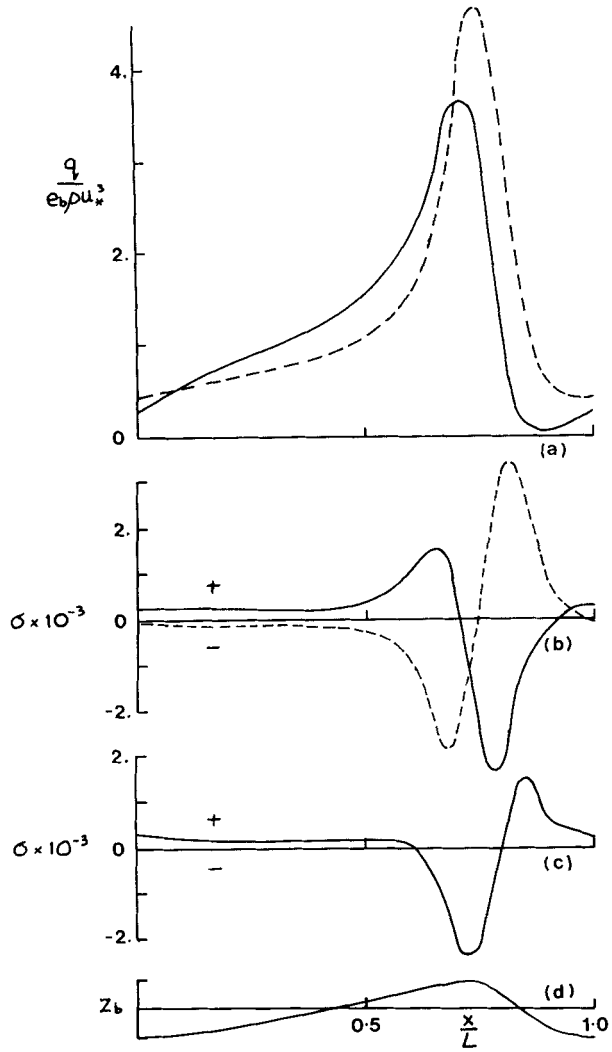

Figure 9. Bed-load transport over asymmetric wave (3); $D/z_0 = 1600$, $L/D = 6.25$, $a/z_0 = 200$, $\tan\phi = 0.6$. (a)–(d) As in Fig. 7.

increasing and moving downstream with a consequent separation of the flow. The erosion curve for flow in the opposite direction shows deposition occurring at the crest with the crest now moving to the left. Defining

$$T_1 = \int u_*^3 \, dt$$

and

$$T_2 = \int u_*^3 \, dt$$

where the integrals are performed over the time when the flow is with and against the asymmetry respectively the erosion over each part of the tidal cycle is then proportional to

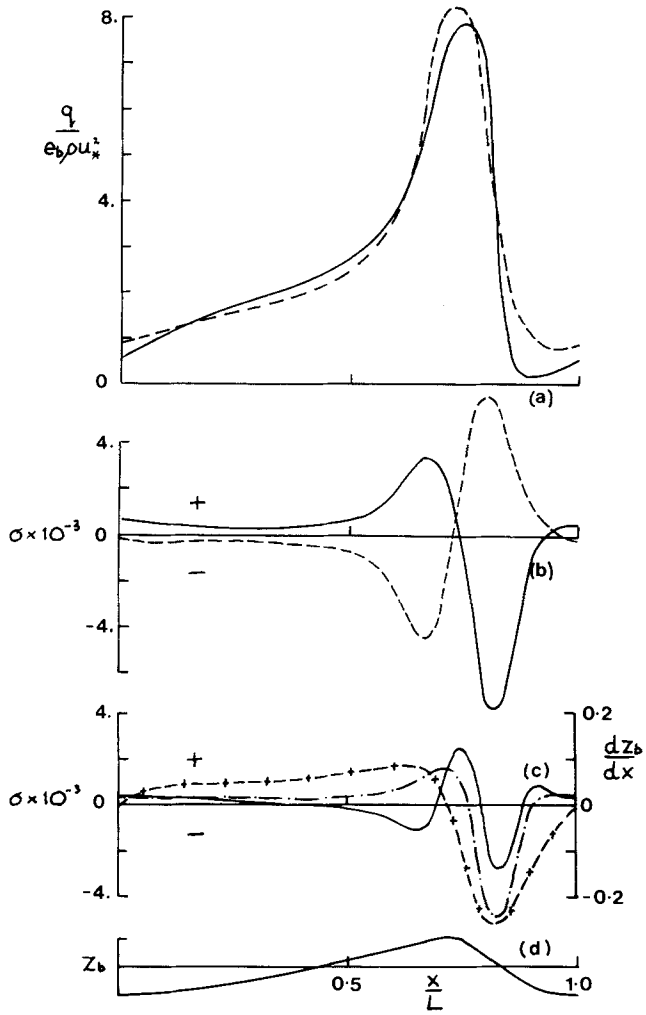

Figure 10. Bed-load transport over asymmetric wave (3). As for Fig. 9 with $\tan\phi = 0.3$. In (c): ——, $T_1 = -T_2$; – · –, $T_1 = 2T_2$; – + –, dz_b/dx.

T_1 and T_2 respectively. The net erosion with $T_1 = -T_2$ is shown in Fig. 9(c). The result would be the wave crest becoming more trochoidal and the lee slope becoming steeper with no movement of the crest and with the flow separating.

With $\tan\phi = 0.3$ (Fig. 10) the flow with the asymmetry produces erosion at the crest whilst deposition occurs when the flow is in the opposite direction. With $T_1 = -T_2$ the net erosion would result in the wave crest decreasing in height and moving to the left, the wave assuming a more symmetric form. With $T_1 = -2T_2$ a maximum erosion occurs just upstream of the crest and a maximum deposition halfway down the lee slope. This would lead to an advancement of the crest with the crest becoming more rounded and a steepening of the lower half of the lee slope.

For a wave to remain constant in shape and to progress at a constant velocity, c, we require that

$$z_b = z_b(x - ct).$$

From equation (5.2) and taking $t = 0$ this leads to the requirement

$$\frac{\partial q_b}{\partial x} = c(1-n)\frac{\partial z_b}{\partial x}. \tag{5.4}$$

Thus the net erosion should be proportional to the slope of the underlying wave. The slope of the bed wave, $\partial z_b/\partial x$, is plotted in Fig. 10(c). Comparing this curve with the net erosion curve for $T_1 = -2T_2$ with $\tan\phi = 0.3$ we find that neither the erosion on the stoss slope nor the deposition on the lee slope are large enough for the wave to propagate without change in shape. As a rough estimate, however, for the propagation speed c of the wave by comparing the amplitudes of the two curves we obtain $c \sim 0.2$ m day^{-1} (here we have taken $u_* = 0.4$ cm s^{-1}, $e_b = 0.1$ and $z_0 = 0.5$ cm). This value compares well with observed rates of advance of sand waves (see Taylor & Dyer 1977).

6 Comparison with data from the Columbia River

A series of field experiments have been conducted by J. D. Smith of the University of Washington and his co-workers between 1968 and 1972 in the Columbia River. Flow measurements were taken over sandwaves ranging from 75 to 100 m in length and 1.5 to 3.0 m high in flow depths of approximately 15 m. The crest lines of individual waves had a certain degree of curvature, although this was slight and we expect our assumption of two-dimensionality to hold, at least to the accuracy of the measurements. Of the experiments the most extensive was carried out in 1972 and reported by McLean (1976). The turbulence measurements are described in McLean & Smith (1979). To reduce the effect of unresolvable faster moving megaripples six waves considered of similar shape in the 1972 data were combined into a single composite wave and an ensemble mean taken of the flow data.

We shall consider two wave profiles reported by McLean (1976), labelled 1972 Wave 1 (the composite wave, see Fig. 11) and 1969 Wave 1 (Fig. 13). No direct measurements of surface shear stress were taken. McLean estimates the friction velocity, $(\tau/\rho)^{1/2}$ from the lowest mean velocity measurement and an estimate for z_0. McLean's fit to the data for the two waves is shown in Figs 11 and 13.

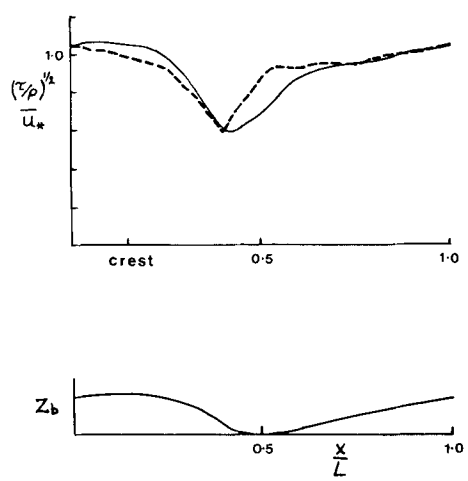

Figure 11. Friction velocity, $(\tau/\rho)^{1/2}$, and wave profile for 1972 Wave 1 (McLean 1976): – – –, measured; ——, model prediction.

The parameters for 1972 Wave 1 are $D/z_0 = 1580$ and $L/D = 6.4$ and we shall take $Fr = 0$. The bed profile is defined by 20 equally spaced data points across the bed elevation given in Fig. 11. The maximum wave slope is 0.12. The model was run with the above parameters on a 20×14 grid. For this particular run no aliasing errors were produced and no filtering of the bed form data was required.

The model results for $(\tau/\rho)^{1/2}$ are given in Fig. 11. The value of u_*, the undisturbed friction velocity, has been estimated for McLean's data by requiring that the means of the two curves are equal. The form drag of the wave was 7 per cent of the total, a surprisingly low value. The shape of the predicted curve for $(\tau/\rho)^{1/2}$ is very similar to the results of McLean with a minimum in $(\tau/\rho)^{1/2}$ at $x/L = 0.42$ compared with 0.39 from McLean's data. The model gives a maximum at $x/L = 0.08$. McLean's data do not show a distinct maximum although true perodicity would clearly demand one. As a measure of the variability of shear stress over the wave we define

$$V = \frac{\tau_{\max} - \tau_{\min}}{\frac{1}{2}(\tau_{\max} + \tau_{\min})}.$$

The model results give a value of $V = 1.00$ whilst McLean's results give $V = 0.92$.

The erosion rate, σ (equation 5.3), predicted by the model from equation (5.2) is shown in Fig. 12. Because of the high shear stress reported during the experiments we shall take $\tan\phi = 0.3$. This gives a maximum deposition halfway down the lee slope at $x/L = 0.36$ and a maximum erosion just downstream of the trough at $x/L = 0.56$. Also plotted on Fig. 12 is the slope of the bed wave, dz_b/dx. From equation (5.4) the bed wave will progress forward without change in shape if $\sigma \propto dz_b/dx$. Fig. 12 shows a good correspondence between the phases and ratio of the maxima and minima of σ and dz_b/dx. The wave is therefore approximately progressive without change in amplitude and, taking $u_* = 4$ cm s^{-1} has a forward velocity of approximately 1.5 m day^{-1}. This compares with a reported 5 m day^{-1} for the observed sand wave field as a whole.

The parameters for 1969 Wave 1 (Fig. 13) are $D/z_0 = 11360$ and $L/D = 4.67$. The lee slope is somewhat steeper than 1972 Wave 1 with a maximum slope of 0.36. With these values of the parameters and a 20 data point representation of the bed form the solution was found to oscillate at a two-grid interval wavelength. Filtering the bed-wave data points using equations (3.3) and reducing D/z_0 to 1136 reduced this oscillation to a small fraction of the total perturbation. The maximum difference between the original data points and the filtered points after six passes of the filter was approximately 2 per cent. The distribution

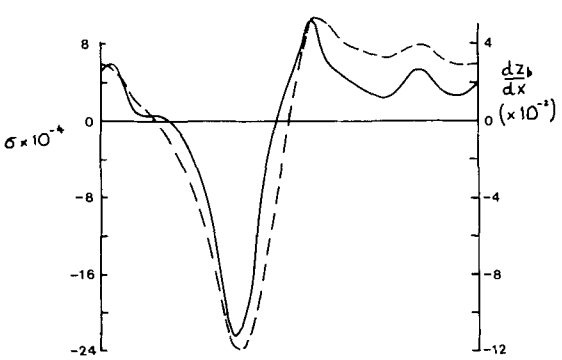

Figure 12. Erosion rate predicted by the model for 1972 Wave 1 and bed wave shape: ——, erosion rate; – – –, dz_b/dx.

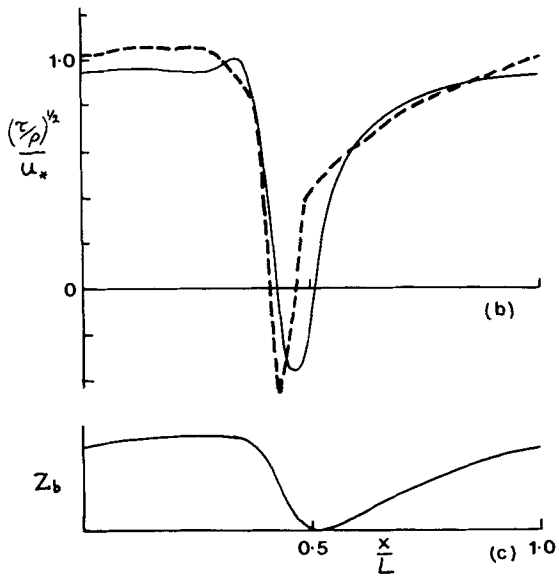

Figure 13. Friction velocity $(\tau/\rho)^{1/2}$, and wave profile for 1969 Wave 1 (McLean 1976): – – –, measured; ——, model prediction.

of $(\tau/\rho)^{1/2}$ predicted by the model is shown in Fig. 13. The negative shear stress shows the mean flow to separate. The form drag was 22 per cent of the total. Comparing this with the $(\tau/\rho)^{1/2}$ distribution by McLean again gives good agreement. The position of the minimum given by the model is $x/L = 0.47$ whilst McLean's results show a minimum at $x/L = 0.44$. The models results give a value of $V = 4.06$. McLean's results give $V = 3.1$. The position and length of the separation bubble in the two cases also compares well, with the length being $x/L = 0.08$ for the model and $x/L = 0.06$ for McLean's results. The position of the bubble is marginally lower on the lee slope for the model compared with McLean's results.

The slope of the lee face of the wave is close to the angle of repose of the bed material. This, together with the separation of the flow, makes an examination of the bed load and erosion rate using equations (5.1) and (5.2) inappropriate. However, the stress distribution given in Fig. 13 suggests a slight flattening of the wave just above the lee slope and a forward movement of the lee face.

The model shows a large variation of the position of the stress maximum with height above the wave, similar to that found by Taylor *et al.* (1976). For 1972 Wave 1 the results give at $z/z_0 = 37$ the maximum at $x/L = 0.15$ increasing to $x/L = 0.5$ at $z/z_0 = 225$. Above this height the phase of the stress maximum remains approximately constant with height. The phase shift of the turbulent energy

$$E = \frac{1}{2} \sum_{i=1}^{3} u_i'^2$$

is similar to that predicted for the shear stress. Note that the height $z/z_0 = 225$ is less than the height $s/z_0 = 510$, calculated from equation (2.5), at which we would expect our turbulence closure scheme to become invalid.

The averaged measurements of $\overline{u'^2}$ and $\overline{w'^2}$ over the composite 1972 Wave 1 reported in McLean & Smith (1979) clearly show a phase shift from approximately $x/L = 0.12$ at $z/z_0 = 37$ to 0.5 at $z/z_0 = 225$ agreeing well with the phase shift of E predicted by the model.

The measurements of shear stress, $-\rho\overline{u'w'}$, however, do not show such a large phase shift. Over the interval $37 < z/z_0 < 225$ the phase of the shear stress is approximately constant with height, the stress maximum at approximately $x/L = 0.4$. It should be noted that there was a large degree of scatter in the measured turbulence quantities, particularly in the lower values of the shear stress.

7 Discussion

Dunes formed in uni-directional flows, such as flumes and rivers, are asymmetric with often avalanche lee slopes where the angle of the lee slope is equal to the angle of repose of the sand grains (about 30°). The crest is often sharp and separation of the flow takes place. This, however, is not always the case for dunes in large rivers. The results for 1972 Wave 1 from the Columbia River data suggest that progressive waves are possible without the flow separating. Sand waves observed in the sea, however, seldom have slopes exceeding 0.17 (10°). The steepness of the wave ($2a/L$) is typically 1/30 ($ak = 0.1$). For sand waves in the sea with rounded crests and with a ratio of $L/D = 6.25$ using Fig. 3 and Tables 4 and 5 we conclude that the flow will be non-separating. For larger values of L/D the flow becomes closer to separating with the possibility of separation occurring over the very steep waves (see Fig. 2). For a sine wave and $L/D = 12.5$ this occurs at $ak = 0.17$. For the sharper crested waves (2) and (3) we would expect separation to occur at lower values of ak (approximately $ak \simeq 0.1$ for the asymmetric wave) with maximum slopes of about 0.2. The shape of the crest will also be important. Sand waves often have trochoidal shaped crests and again we may expect separation to occur at the crest for the very sharply crested waves at lower values of ak.

With the three analytic bed forms considered we can only obtain a limited amount of information about the fully developed bed waves to form in a given flow. However, the results do show some interesting features with a dependence of the wave-shape on the value of $\tan\phi$ and the ratio T_1/T_2. We would also expect the shape to depend on the variation of e_b with τ. We obtained a stable wave form only for the symmetric wave with $\tan\phi = 0.3$. The steepness of the wave, 1/25, compares well with observed bed waves. The flow over the wave in this case was non-separating. It is not clear from the present results whether or not the symmetric wave with $\tan\phi = 0.6$ or the asymmetric wave developing from a small perturbation of the bed will reach a steady form before separation of the flow takes place.

The results for the symmetric wave with $\tan\phi = 0.3$ and steepness 1/25 show a different behaviour for the sine wave, which increases in steepness, from that for the $\sin^4$ wave which is approximately stable. This suggests that the past history of the bed wave and flow conditions may be important in determining its shape with there being more than one stable bed form for given flow and bed conditions.

The model predicts that the shape of the crest is dependent on the value of $\tan\phi$ and thus on the value of shear stress. For decreasing $\tan\phi$, i.e. increasing shear, the crest of the sand wave will become flatter. A flattening of the crest as the shear stress increases has been observed for a sand-wave in the sea (D. N. Longhome, private communication) with the crest being sharper during neap tides (low u_*) than spring tides (high u_*). Harvey & Vincent (1977) report a decrease in the value of the effective z_0 of a rippled bed (and therefore flattening of the ripples) as the shear stress increases.

Acknowledgments

Most of the work described in this paper was undertaken while the authors were in the Department of Oceanography, University of Southampton. Their work there was supported

by the NERC through a studentship to KJR and through grant GR3/3014. We are grateful to Rick Nunes for assistance with some of the calculations and to Keith Dyer and Nick Langhorne of I.O.S. Taunton for their advice and encouragement.

References

Allen, J. R. L., 1968. *Current Ripples,* North-Holland.

Bagnold, R. A., 1954. Experiments on the gravity-free dispersion of large spheres in a Newtonian fluid under shear, *Proc. R. Soc.,* **225A**, 49.

Bagnold, R. A., 1966. An approach to the sediment transport problem from general physics, *U.S. Geol. Surv., Prof. Pap., 422–21.*

Blackadar, A. K., 1962. The vertical distribution of wind and turbulent exchange in a neutral atmosphere, *J. geophys. Res.,* **67**, 3095–3102.

Britter, R. E., Hunt, J. C. R. & Richards, K. J., 1981. Air flow over a two-dimensional hill: studies of velocity speed-up, roughness effects and turbulence, *Q. J. R. Met. Soc.,* **107**, 91–110.

Chorin, A. J., 1967. A numerical method for solving incompressible viscous flow problems, *J. Comp. Phys.,* **2**, 12–26.

Exner, F. M., 1925. Über die Wechselwirkung zwischen Wasser und Geschiebe in Flüssen, *Sitzber-Akad. Wiss (Wien),* **3–4**, 165–180.

Gent, P. R. & Taylor, P. A., 1976. A numerical model of air flow above water waves, *J. Fluid Mech.,* **77**, 105–128.

Harvey & Vincent, 1977. Observations of shear in near-bed currents in the Southern N. Sea, *Est. coastal Mar. Sci.,* **5**, 715–731.

Inman, D. L., 1963. In *Submarine Geology,* chapter V, 2nd edn, ed. Shepard, F. P., Harper & Row, New York.

Langeraar, W., 1966. Sand waves in the North Sea, *Hydrogr. Newslett.,* **1**, 243–246.

McLean, S. R., 1976. Mechanics of the turbulent boundary layer over sand waves in the Columbia River, *PhD thesis,* University of Washington.

McLean, S. R. & Smith, J. D., 1979. Turbulence measurements in the boundary layer over a sand wave field, *J. geophys. Res.,* **84**, 7791–7808.

Richards, K. J., 1978. Theoretical models for the formation and development of sand and gravel waves, *PhD thesis,* University of Southampton.

Richards, K. J., 1980. The formation of ripples and dunes on an erodible bed, *J. Fluid Mech.,* **99**, 597–618.

Roach, P. J., 1972. *Computational Fluid Dynamics,* Hermosa, Albuquerque, New Mexico, 434 pp.

Shapiro, R., 1970. Smoothing, filtering and boundary effects, *Rev. Geophys. Space Phys.,* **8**, 359–387.

Taylor, P. A., 1977. Some numerical solutions of surface boundary-layer flows above gentle topography, *Boundary-Layer Meteorol.,* **11**, 439–465.

Taylor, P. A. & Dyer, K. R., 1977. Theoretical models of flow near the bed and their implications for sediment transport, in *The Sea,* **6**, 579–601, ed. Goldberg, E. D., Wiley, London.

Taylor, P. A., Gent, P. R. & Keen, J. M., 1976. Some numerical solutions for turbulent boundary-layer flow above fixed rough, wavy surfaces, *Geophys. J. R. astr. Soc.,* **44**, 177–201.

Taylor, P. A., Richards, K. J. & Nunes, R. A., 1978. Models of turbulent airflow above idealised water waves, in *Turbulent Fluxes through the Sea Surface, Wave Dynamics and Predictions,* eds Faure, A. & Hasselmann, Klaus, Plenum, New York.

Van Veen, J., 1935. Sand waves in the Southern North Sea, *Natl. Hydrogr. Rev.,* **12**, 229.

Appendix

We shall derive conservative forms for the finite difference representations of the flow divergence and advection terms in the non-orthogonal coordinate system (x^*, z^*).

First let us consider the divergence of flow, $\nabla \cdot \mathbf{U}$ which in (x^*, z^*) coordinates is

$$\nabla \cdot \mathbf{U} = \frac{\partial U}{\partial x^*} + \left(\frac{\partial U}{\partial z^*} \frac{\partial z^*}{\partial x} + \frac{\partial W}{\partial z^*} \frac{\partial z^*}{\partial z} \right). \tag{A1}$$

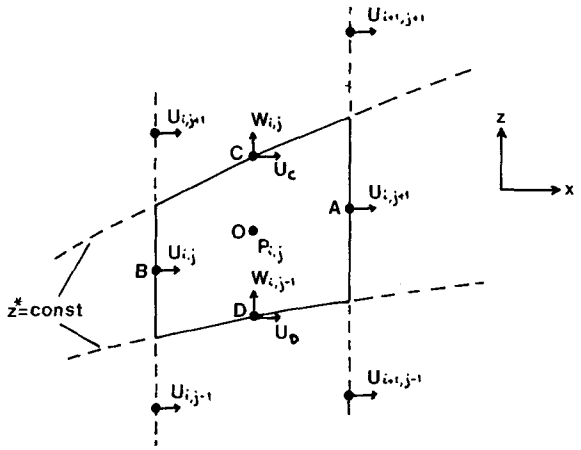

Figure A1. Control volume for the evaluation of the divergence term.

We shall use a control volume approach. The (i, j)th mesh cell in the Cartesian plane (x, z) is shown in Fig. A1. The sides of the cell are given by the lines of constant x^* and z^*.

The divergence of the flow in the cell can be represented by the sum

$$\mathrm{DIV}_{i,j} = \mathrm{DIV}\ U + \mathrm{DIV}\ W \tag{A2}$$

where

$$\mathrm{DIV}\ U = \left[U_{i,j+1} \cdot \frac{\partial z}{\partial z^*}\bigg|_A - U_{i,j} \cdot \frac{\partial z}{\partial z^*}\bigg|_B\right] \frac{1}{\Delta x^*} \cdot \frac{\partial z^*}{\partial z}\bigg|_0$$

and

$$\mathrm{DIV}\ W = \left[\left\{W_{i,j} - U_C \frac{\partial z}{\partial x}\bigg|_C\right\} - \left\{W_{i,j-1} - U_D \frac{\partial z}{\partial x}\bigg|_D\right\}\right] \frac{1}{\Delta z^*} \frac{\partial z^*}{\partial z}\bigg|_0.$$

The derivatives $\partial z/\partial x$ are taken along $z^* = \text{constant}$ and the terms U_C and U_D can be represented by

$$U_C = \tfrac{1}{4}\left[U_{i,j} + U_{i+1,j} + U_{i,j+1} + U_{i+1,j+1}\right]$$

$$U_D = \tfrac{1}{4}\left[U_{i,j} + U_{i+1,j} + U_{i,j-1} + U_{i+1,j-1}\right].$$

Taking $z^* = \text{constant}$ we have

$$\frac{\partial z^*}{\partial x} + \frac{\partial z^*}{\partial z} \cdot \frac{\partial z}{\partial x}\bigg|_{z^*} = 0$$

and hence the derivative

$$\frac{\partial z}{\partial x}\bigg|_{z^*} = -\frac{\partial z^*/\partial x}{\partial z^*/\partial z}.$$

For a given coordinate transformation the derivatives $\partial z^*/\partial x$, $\partial z^*/\partial z$ etc. can be determined explicitly at each grid point of the cell.

It can be easily shown that

$$\lim_{\Delta x^*, \Delta z^* \to 0} \mathrm{DIV}_{i,j} = \nabla \cdot \mathbf{U}.$$

The above scheme is conservative in (x^*, z^*) coordinates, i.e.

$$S = \sum_{\text{all } i,j} \text{DIV}_{i,j} \equiv 0.$$

The equations are solved in (x^*, ζ) space where S is not identically zero. However, for a typical run using a 10×10 grid, after 2000 time steps $S \sim 10^{-11}$, where individual $\text{DIV}_{i,j} \sim 10^{-10}$ which was considered to be small enough. Attempts to use a conservative form $\text{DIV}^*_{i,j} = \text{DIV}_{i,j}/(\partial\zeta/\partial z|_0)$ where now $S^* \equiv 0$ caused the numerical scheme to become unstable for the same time step.

The U advection terms in (x^*, z^*) space, namely

$$\text{AD}U = U\frac{\partial U}{\partial x^*} + \left(U\frac{\partial z^*}{\partial x} + W\frac{\partial z^*}{\partial z}\right)\frac{\partial U}{\partial z^*}$$

using the continuity equation can be written in the form

$$\text{AD}U = \frac{\partial z^*}{\partial z}\left[\frac{\partial}{\partial x^*}\left(U^2\frac{\partial z}{\partial z^*}\right) + \frac{\partial}{\partial z^*}\left(U^2\frac{\partial z^*/\partial x}{\partial z^*/\partial z} + U\cdot W\right)\right].$$

We shall again use a control volume approach. Taking a control volume centred on $U_{i,j}$ (Fig. A2) an appropriate finite difference representation is

$$\text{AD}U = \frac{1}{4\Delta x^*}\frac{\partial z^*}{\partial z}\bigg|_0 \left[(U_{i,j} + U_{i+1,j})(UN_{i,j} + U_{i+1,j})\frac{\partial z}{\partial z^*}\bigg|_E \right.$$

$$\left. - (U_{i,j} + U_{i-1,j})(UN_{i,j} + U_{i-1,j})\frac{\partial z}{\partial z^*}\bigg|_F\right]$$

$$+ \frac{1}{2\Delta z^*}\frac{\partial z^*}{\partial z}\bigg|_0 [W1UP(UN_{i,j} + UN_{i,j+1}) - W1D(UN_{i,j} + UN_{i,j-1})]$$

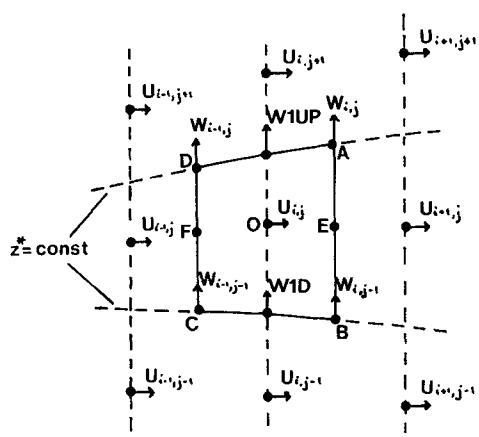

Figure A2. Control volume for the evaluation of the advection term.

where

$$W1UP = \frac{1}{2}\left[\frac{1}{4}\left.\frac{\partial z^*/\partial x}{\partial z^*/\partial z}\right|_{\mathrm{B}} (U_{i,j} + U_{i,j+1} + U_{i-1,j} + U_{i-1,j+1}) + \frac{1}{4}\left.\frac{\partial z^*/\partial x}{\partial z^*/\partial z}\right|_{\mathrm{A}} (U_{i,j} + U_{i,j+1} + U_{i+1,j} + U_{i+1,j+1})\right] + \frac{1}{2}[W_{i,j} + W_{i-1,j}]$$

$$W1D = \frac{1}{2}\left[\frac{1}{4}\left.\frac{\partial z^*/\partial x}{\partial z^*/\partial z}\right|_{\mathrm{C}} (U_{i,j} + U_{i,j-1} + U_{i-1,j} + U_{i-1,j+1}) + \frac{1}{4}\left.\frac{\partial z^*/\partial x}{\partial z^*/\partial z}\right|_{\mathrm{D}} (U_{i,j} + U_{i,j-1} + U_{i+1,j} + U_{i+1,j-1})\right] + \frac{1}{2}[W_{i,j-1} + W_{i-1,j-1}]$$

and $UN_{i,j}$ denotes the updated value $U_{i,j}$ etc. The advection terms in the E and W equations are treated similarly.

The above scheme is conservative in momentum in (x^*, z^*) space. However, because of the expanded vertical coordinate we cannot represent them in a truely conservative manner in (x^*, ζ) space (see, e.g. Roach 1972, p. 281).